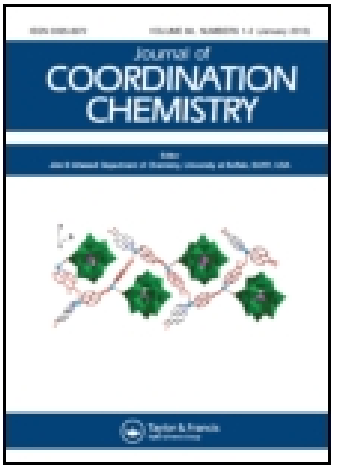

Journal of Coordination Chemistry
Publication details, including instructions for authors and subscription information:
http://www.tandfonline.com/loi/gcoo20

Syntheses, structures, and photocatalysis of five inorganic-organic hybrid compounds constructed from Keggin polyoxometalate clusters and multidentate N-donor ligands

Wei-Qiu Kan[a], Ji-Ming Xu[a], Yu-He Kan[a], Jiao Guo[c] & Shi-Zheng Wen[ab]

[a] School of Chemistry and Chemical Engineering, Huaiyin Normal University, Huaian, PR China

[b] School of Physics and Electronic Electrical Engineering, Huaiyin Normal University, Huaian, PR China

[c] College of Chemistry and Chemical Engineering, Xinxiang University, Xinxiang, PR China

Accepted author version posted online: 13 Jan 2014.Published online: 27 Feb 2014.

To cite this article: Wei-Qiu Kan, Ji-Ming Xu, Yu-He Kan, Jiao Guo & Shi-Zheng Wen (2014) Syntheses, structures, and photocatalysis of five inorganic-organic hybrid compounds constructed from Keggin polyoxometalate clusters and multidentate N-donor ligands, Journal of Coordination Chemistry, 67:2, 195-214, DOI: 10.1080/00958972.2014.882503

To link to this article: http://dx.doi.org/10.1080/00958972.2014.882503

Journal of Coordination Chemistry, 2014
Vol. 67, No. 2, 195–214, http://dx.doi.org/10.1080/00958972.2014.882503

Syntheses, structures, and photocatalysis of five inorganic–organic hybrid compounds constructed from Keggin polyoxometalate clusters and multidentate N-donor ligands

WEI-QIU KAN†, JI-MING XU*†, YU-HE KAN†, JIAO GUO§ and SHI-ZHENG WEN*†‡

†School of Chemistry and Chemical Engineering, Huaiyin Normal University, Huaian, PR China
‡School of Physics and Electronic Electrical Engineering, Huaiyin Normal University, Huaian, PR China
§College of Chemistry and Chemical Engineering, Xinxiang University, Xinxiang, PR China

(*Received 25 September 2013; accepted 30 December 2013*)

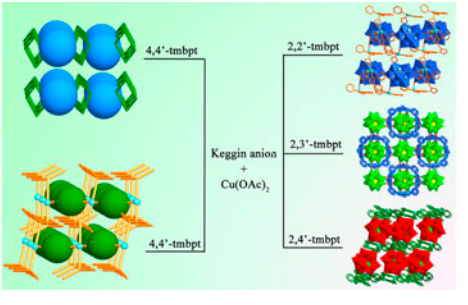

Five inorganic–organic hybrid compounds have been synthesized, and the photocatalytic properties of the compounds have also been studied.

Five inorganic–organic hybrid compounds have been prepared under hydrothermal conditions and characterized by single-crystal X-ray diffraction analyses, infrared spectra, elemental analyses, powder X-ray diffraction, and thermogravimetric analyses. In **1**, each 2,2′-tmbpt ligand links two Cu(II) ions to generate a highly undulated chain. The chains are further bridged by $[SiW_{12}O_{40}]^{4-}$ anions to form a layer. Compound **2** exhibits a 3-D (3,4,5)-connected framework with large channels, in which $[SiW_{12}O_{40}]^{4-}$ anions are tetradentate linkages. In **3**, each 2,4′-tmbpt links three Cu(II) ions to form 2-D layers, which are further linked by $[SiW_{12}O_{40}]^{4-}$ to yield a 3-D (3,4)-connected framework. In **4**, each 4,4′-tmbpt connects three Cu(II) ions to generate 1-D double chains. In **5**, $[PW_{12}O_{40}]^{3-}$ link Cu(II) ions to generate 1-D chains. Compounds **1**–**5** exhibit photocatalytic activities for degradation of methylene blue and rhodamine B.

*Corresponding authors. Email: xujm68@126.com (J.-M. Xu); szwen@hytc.edu.cn (S.-Z. Wen)

Keywords: Polyoxometalates; Multidentate N-donor ligand; Inorganic–organic hybrid; Topological analyses; Photocatalysis

1. Introduction

Polyoxometalates (POMs), as one kind of metal-oxide cluster with nanosizes, diverse topologies and potential applications in catalysis, ion exchange, electrical conductivity, magnetism, photochemistry, and antibacterial agent, have drawn much attention [1]. The design and synthesis of new POM-based compounds through modification of different transition metal complexes is a remarkable branch of POMs chemistry [2]. In these POM-based compounds, the polyoxoanions serve as inorganic linkages, providing terminal/bridging oxygens [3], or only act as inorganic templates, without utilizing the coordination ability of terminal/bridging oxygens [4].

Choice of ligand is important in coordination polymers [5]. N-donor ligands with strong coordination capacity have been used for the construction of modified POM-based compounds [6]. Rigid N-donors, such as 2,2′-bipyridine, 4,4′-bipyridine, and 5,6-diamino-1,10-phenanthroline, have been extensively used for preparation of POM-based compounds because of their conformational transformation and controllable structures [5, 7]. Recently, flexible ligands, such as bis(imidazole) and bis(triazole), have been utilized to synthesize POM-based compounds with fascinating architectures. These flexible ligands exhibit conformational freedom, which allow them to conform to the coordination requirements of metal ions for construction of high-dimensional frameworks with various topologies [5, 8].

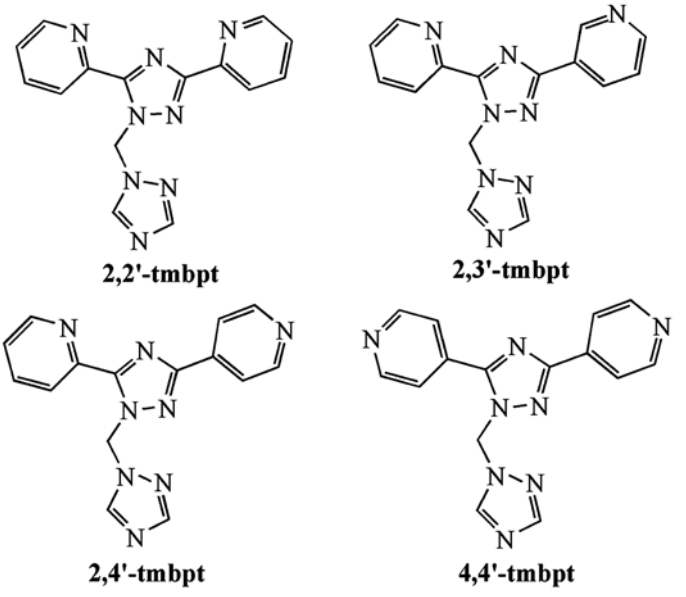

Scheme 1. The multidentate N-donors used in this work.

Most of the previously reported POM-based compounds are constructed by bidentate ligands, with multidentate N-donor ligands rarely observed [7–9].

In this work, the multidentate N-donor ligands 1-((1*H*-1,2,4-triazol-1-yl)methyl)-3,5-bis(pyridyl)-1,2,4-triazole (scheme 1) were employed for the following considerations: (i) they contain two rigid pyridyl groups and one flexible –(CH_2)– group, which have the merits of both rigid and flexible ligands, and (ii) they have six potential metal-binding sites and can provide diverse coordination modes. Here, five compounds based on Keggin polyanions, Cu(II), and multidentate N-donor ligands, $[Cu_2(2,2'\text{-tmbpt})_2(SiW_{12}O_{40})]\cdot 9H_2O$ (**1**), $Cu_2(2,3'\text{-tmbpt})_2(SiW_{12}O_{40})]\cdot 6H_2O$ (**2**), $[Cu_2(2,4'\text{-tmbpt})_2(SiW_{12}O_{40})(H_2O)_2]\cdot 6.5H_2O$ (**3**), $[Cu_2(4,4'\text{-tmbpt})_2(SiW_{12}O_{40})(H_2O)_4]\cdot 13.5H_2O$ (**4**), and $[Cu(4,4'\text{-Htmbpt})(4,4'\text{-tmbpt})(PW_{12}O_{40})(H_2O)_2]\cdot 7H_2O$ (**5**), where 2,2′-tmbpt = 1-((1*H*-1,2,4-triazol-1-yl)methyl)-3,5-bis(2-pyridyl)-1,2,4-triazole, 2,3′-tmbpt = 1-((1*H*-1,2,4-triazol-1-yl)methyl)-3-(3-pyridyl)-5-(2-pyridyl)-1,2,4-triazole, 2,4′-tmbpt = 1-((1*H*-1,2,4-triazol-1-yl)methyl)-3-(4-pyridyl)-5-(2-pyridyl)-1,2,4-triazole and 4,4′-tmbpt = 1-((1*H*-1,2,4-triazol-1-yl)methyl)-3,5-bis(4-pyridyl)-1,2,4-triazole, have been prepared under hydrothermal conditions. These compounds have been characterized by single-crystal X-ray diffraction analyses, infrared spectra (IR), elemental analyses, powder X-ray diffraction (PXRD), and thermogravimetric analyses (TGA). The optical band gaps of the compounds have been investigated. Compounds **1**–**5** exhibit photocatalytic activities for degradation of methylene blue (MB) and rhodamine B (RhB) under UV light irradiation and show good stabilities toward UV light photocatalysis.

2. Experimental

2.1. *Materials and methods*

The tmbpt ligands were synthesized by reported procedures [10]. All other reagents were purchased from commercial sources and used without purification. A Perkin-Elmer 240 elemental analyzer was used to collect microanalytical data. A Mattson Alpha-Centauri spectrometer was used to collect FT-IR spectra data, which were recorded as KBr pellets from 4000 to 400 cm^{-1}. TGA of **1**–**5** were carried out on a Perkin-Elmer TG-7 analyzer heated from room temperature to 800 °C under nitrogen. PXRD patterns of **1**–**5** were collected on a Rigaku Dmax 2000 X-ray diffractometer with graphite-monochromated Cu-Kα radiation ($\lambda = 0.154$ nm and 2θ ranging from 5° to 50°. Diffuse reflectance spectra were recorded on a Cary 500 spectrophotometer equipped with a 110 mm diameter integrating sphere from 200 to 800 nm. Photocatalytic experiments were carried out in conventional processes. A suspension containing **1**–**5** (30 mg) and 200 mL MB (5×10^{-5} M L^{-1}) or RhB solution (4×10^{-5} M L^{-1}) was stirred in the dark for 30 min to establish adsorption equilibrium before irradiation. It was then stirred continuously under a 125 W Hg lamp. Every 15 min, 3 mL of samples were taken out of the reactor and separated through centrifuge to remove suspended catalyst particles and then subjected to spectroscopic measurement on the UV–Vis spectrometer. The concentrations of MB and RhB were estimated by the absorbances at 665 and 557 nm, which directly relate to the structural change of the chromophore. The pH values of all the reaction systems were about 6.5, and changes were not observed after the catalytic processes.

Table 1. Crystal data and structure refinements for **1**–**5**.[a,b]

	1	**2**	**3**	**4**	**5**
Formula	$C_{30}H_{42}Cu_2N_{16}O_{49}SiW_{12}$	$C_{30}H_{36}Cu_2N_{16}O_{46}SiW_{12}$	$C_{30}H_{41}Cu_2N_{16}O_{48.5}SiW_{12}$	$C_{30}H_{59}Cu_2N_{16}O_{57.5}SiW_{12}$	$C_{30}H_{43}CuN_{16}O_{49}PW_{12}$
fw	3772.17	3718.12	3763.16	3925.3	3712.51
Crystal system	Monoclinic	Tetragonal	Monoclinic	Orthorhombic	Triclinic
Space group	*Pc*	*P4/ncc*	$P2_1/n$	*Pnma*	*P–1*
a (Å)	12.8679(3)	26.2444(4)	18.0334(12)	22.8645(6)	11.9999(5)
b (Å)	16.4521(4)	26.2444(4)	17.4912(11)	23.8954(5)	14.3992(5)
c (Å)	17.3925(4)	19.1620(5)	23.409(2)	14.2051(3)	20.8142(8)
α (°)	90	90	90	90	95.634(3)
β (°)	104.763(3)	90	109.440(9)	90	99.522(3)
γ (°)	90	90	90	90	103.801(3)
V (Å^3)	3560.51(15)	13198.2(4)	6962.9(9)	7761.0(3)	3408.8(2)
Z	2	8	4	4	2
D_{Calcd} (g/cm^{-3})	3.519	3.742	3.590	3.359	3.617
GOF on F^2	1.038	1.189	1.018	1.017	1.049
R_1[a] [$I > 2\sigma(I)$]	0.0297	0.0608	0.0367	0.0351	0.0656
wR_2[b] [$I > 2\sigma(I)$]	0.0623	0.1261	0.0660	0.0678	0.1478
R_{int}	0.0270	0.0495	0.0414	0.0551	0.0461

[a]$R_1 = \Sigma||F_o| - |F_c||/\Sigma|F_o|$.
[b]$wR_2 = |\Sigma w(|F_o|^2 - |F_c|^2)|/\Sigma|w(F_o^2)^2|^{1/2}$.

2.2. *Syntheses of complexes*

2.2.1. Synthesis of $[Cu_2(2,2'\text{-tmbpt})_2(SiW_{12}O_{40})]\cdot 9H_2O$ (1). A mixture of 2,2′-tmbpt (0.03 g, 0.1 mM), $Cu(CH_3COO)_2\cdot H_2O$ (0.06 g, 0.3 mM), $H_4SiW_{12}O_{40}\cdot 14H_2O$ (0.288 g, 0.1 mM), and water (8 mL) was stirred for 1 h in air. The pH was then adjusted to 2 with 1 M HCl, and the mixture was transferred to a 15 mL Teflon-lined reactor, which was heated at 130 °C for three days. After the mixture had been cooled to room temperature at 10 °C h^{-1}, blue crystals of **1** were obtained in 36% yield based on 2,2′-tmbpt. The final pH of the reaction system was about 3. Anal. Calcd for $C_{30}H_{42}Cu_2N_{16}O_{49}SiW_{12}$ ($M_r = 3772.17$) (%): C, 9.55; H, 1.12; N, 5.94. Found: C, 9.45; H, 1.16; N, 5.83. IR (KBr, cm^{-1}): 3446(w), 3382 (w), 1612(w), 1531(w), 1471(w), 1431(w), 1361(w), 1322(w), 1281(w), 1203(w), 1171(w), 1123(w), 1063(w), 1015(w), 969(m), 921(s), 881(w), 790(s), 748(m), 672(w), 534(w).

2.2.2. Synthesis of $[Cu_2(2,3'\text{-tmbpt})_2(SiW_{12}O_{40})]\cdot 6H_2O$ (2). The preparation of **2** was similar to that of **1** except that 2,3′-tmbpt (0.03 g, 0.1 mM) was used instead of 2,2′-tmbpt and the pH was adjusted to 1. Blue crystals of **2** were obtained in 21% yield based on 2,3′-tmbpt. The final pH of the reaction system was 2.5. Anal. Calcd for $C_{30}H_{36}Cu_2N_{16}O_{46}SiW_{12}$ ($M_r = 3718.12$) (%): C, 9.69; H, 0.98; N, 6.03. Found: C, 9.55; H, 0.92; N, 5.88. IR (KBr, cm^{-1}): 3547(w), 3119(w), 2986(w), 1612(w), 1520(w), 1488(w), 1455(w), 1415(w), 1398(w), 1354(w), 1285(w), 1213(w), 1321(m), 1156(w), 1130(w), 1065(w), 1017(w), 967 (m), 924(s), 880(w), 798(s), 760(s), 748(s), 718(m), 705(m), 669(w).

2.2.3. Synthesis of $[Cu_2(2,4'\text{-tmbpt})_2(SiW_{12}O_{40})(H_2O)_2]\cdot 6.5H_2O$ (3). The preparation of **3** was similar to that of **2** except that 2,4′-tmbpt (0.03 g, 0.1 mM) was used instead of 2,3′-tmbpt and the pH was adjusted to 4. Blue crystals of **3** were obtained in 23% yield based on 2,4′-tmbpt. The final pH of the reaction system was 5. Anal. Calcd for $C_{30}H_{41}Cu_2N_{16}O_{48.5}SiW_{12}$ ($M_r = 3763.16$) (%): C, 9.57; H, 1.10; N, 5.96. Found: C, 9.49; H, 1.01; N, 5.82. IR (KBr, cm^{-1}): 3414(w), 3117(w), 1717(w), 1618(w), 1559(w), 1529(w), 1488(w), 1457(w), 1445(w), 1421(w), 1385(w), 1275(w), 1246(w), 1214(w), 1152(w), 1124(w), 1067(w), 1018(m), 971(m), 876(s), 777(s), 669(m).

2.2.4. Synthesis of $[Cu_2(4,4'\text{-tmbpt})_2(SiW_{12}O_{40})(H_2O)_4]\cdot 13.5H_2O$ (4). The preparation of **4** was similar to that of **3** except that 4,4′-tmbpt (0.03 g, 0.1 mM) was used instead of 2,4′-tmbpt and the pH was adjusted to 3. Blue crystals of **4** were collected in 19% yield based on 4,4′-tmbpt. The final pH of the reaction system was 4. Anal. Calcd for $C_{30}H_{59}Cu_2N_{16}O_{57.5}SiW_{12}$ ($M_r = 3925.3$) (%): C, 9.18; H, 1.52; N, 5.71. Found: C, 9.08; H, 1.38; N, 5.55. IR (KBr, cm^{-1}): 3566(w), 3299(w), 3125(w), 1620(w), 1558(w), 1540(w), 1467(w), 1430(w), 1360(w), 1289(w), 1209(w), 1143(w), 1122(w), 1066(w), 1020(w), 975(m), 924 (s), 850(w), 759(s), 668(w).

2.2.5. Synthesis of $[Cu(4,4'\text{-Htmbpt})(4,4'\text{-tmbpt})(PW_{12}O_{40})(H_2O)_2]\cdot 7H_2O$ (5). The pre paration of **5** was similar to that of **4** except that $H_3[PW_{12}O_{40}]\cdot 12H_2O$ (0.288 g, 0.1 mM) was used instead of $H_4SiW_{12}O_{40}\cdot 14H_2O$ and the pH was adjusted to 1. Green crystals

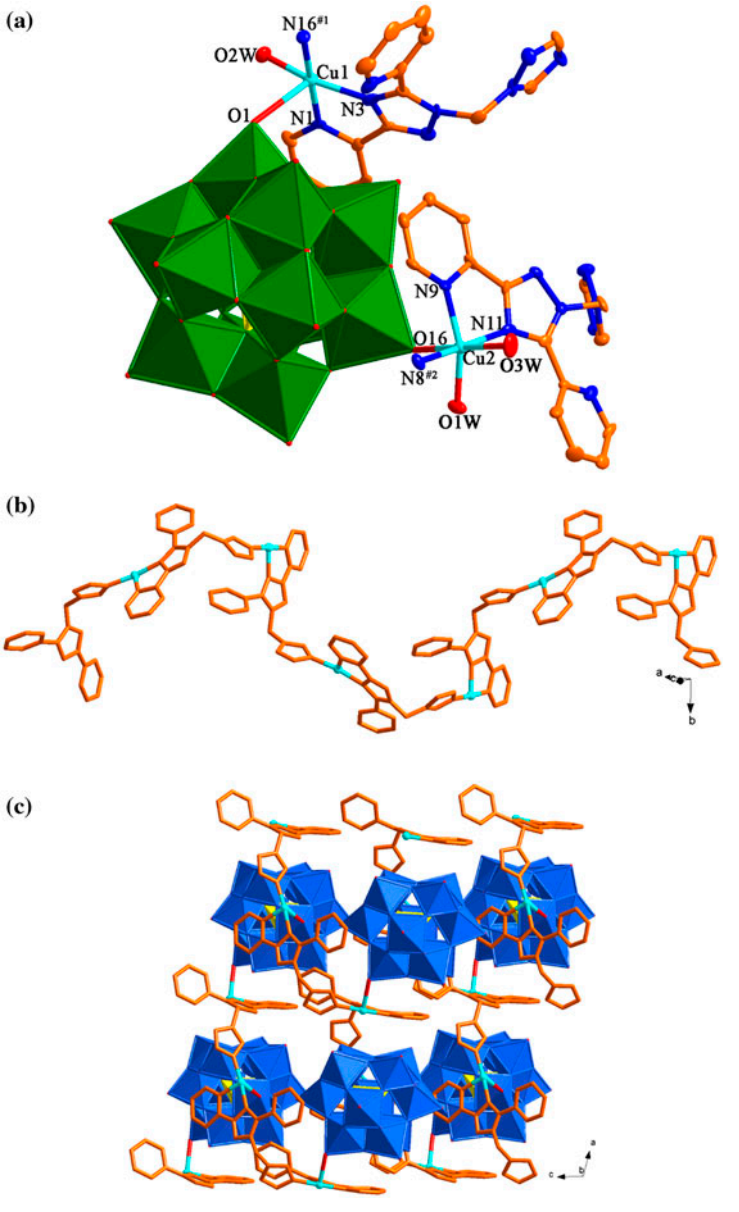

Figure 1. (a) Coordination environments of Cu(II) in **1** with hydrogens and lattice waters omitted for clarity. Symmetry codes: $^{\#1}x$, $-y$, $z+1/2$; $^{\#2}x+1$, y, z. (b) View of the chain formed by Cu(II) and 2,2′-tmbpt. (c) View of the layer of **1**.

of **5** were obtained in 27% yield based on 4,4′-tmbpt. The final pH of the reaction system was 2. Anal. Calcd for $C_{30}H_{43}CuN_{16}O_{49}PW_{12}$ ($M_r = 3712.52$) (%): C, 9.70; H, 1.17; N, 6.04. Found: C, 9.58; H, 1.03; N, 5.95. IR (KBr, cm^{-1}): 3588(w), 3210(w), 3089(w), 1944 (w), 1636(w), 1540(w), 1474(w), 1454(w), 1418(w), 1396(w), 1375(w), 1290(w), 1217(w), 1137(w), 1102(w), 1061(m), 1013(w), 957(s), 881(m), 809(s), 749(s), 704(s), 668(m).

2.3. *X-ray crystallography*

Single-crystal X-ray diffraction data for **1**–**5** were recorded on an Oxford Diffraction Gemini R Ultra diffractometer with graphite-monochromated Mo Kα radiation ($\lambda = 0.71073$ Å) at 293 K. Absorption corrections were applied employing multiscan technique. The structures of **1**–**5** were solved by direct methods of SHELXS-97 [11a] and refined by full-matrix least-squares techniques employing SHELXL-97 [11b]. Non-hydrogen atoms were refined with anisotropic temperature parameters. All hydrogens on carbon and nitrogen were generated geometrically and refined using a riding model with d(C–H) = 0.93 Å, d(N–H) = 0.86 Å, U_{iso}(H) = 1.2U_{eq}(C,N) for aromatic, and d(C–H) = 0.97 Å, U_{iso} = 1.2U_{eq}(C) for CH_2. Water hydrogens were located from difference Fourier maps and refined as riding with d(O–H) = 0.820–0.865 Å and U_{iso}(H) = 1.5U_{eq}(O). Some hydrogens of water were not included in the model. O13, O20, O21, and Si2 of **2** were refined as disordered using O and Si split over two sites with a total occupancy of 1. The detailed crystallographic data and structure refinement parameters of **1**–**5** are summarized in table 1.

3. Results and discussion

3.1. *Description of the crystal structures*

All the polyanions exhibit a classical α-Keggin configuration. Bond lengths and angles of the Keggin polyanions are in the normal ranges as other Cu(II)-containing inorganic–organic hybrid compounds [2e–h, 12].

3.1.1. Structure of $[Cu_2(2,2'\text{-tmbpt})_2(SiW_{12}O_{40})]\cdot 9H_2O$ (1). Compound **1** exhibits a 2-D layer structure. The asymmetric unit of **1** consists of two Cu(II) ions, two 2,2′-tmbpt, one $[SiW_{12}O_{40}]^{4-}$ anion, and nine waters. As shown in figure 1 (a), Cu1 is five-coordinate by three nitrogens from two different 2,2′-tmbpt ligands, two oxygens from one $[SiW_{12}O_{40}]^{4-}$, and one water in a trigonal bipyramidal coordination geometry. Cu2 is six-coordinate by three nitrogens from two 2,2′-tmbpt ligands and three oxygens from one $[SiW_{12}O_{40}]^{4-}$ with two lattice waters in a distorted octahedron. Cu–N and Cu–O bond lengths are 1.956(12)–2.044(17) Å and 1.957(12)–2.784(1) Å, respectively. Each 2,2′-tmbpt links two Cu(II) ions to generate a highly undulated chain [figure 1(b)]. The chains are further bridged by $[SiW_{12}O_{40}]^{4-}$ to form a layer [figure 1(c)].

3.1.2. Structure of $[Cu_2(2,3'\text{-tmbpt})_2(SiW_{12}O_{40})]\cdot 6H_2O$ (2). Compound **2** exhibits an interesting 3-D (3,4,5)-connected framework containing 1-D tube-like chains. The asymmetric unit of **2** consists of one Cu(II), one 2,3′-tmbpt, two kinds of $[SiW_{12}O_{40}]^{4-}$ ($[SiW_{12}O_{40}]^{4-}$-1 and $[SiW_{12}O_{40}]^{4-}$-2), and three lattice waters. As shown in figure 2(a), Cu1 is six-coordinate by two oxygens from one $[SiW_{12}O_{40}]^{4-}$-1 and one $[SiW_{12}O_{40}]^{4-}$-2 anion, and four nitrogens from three 2,3′-tmbpt ligands in an octahedral coordination geometry. The Cu–N bond distances are 2.017(2)–2.053(2) Å and the Cu–O bond lengths are 2.224(1) and 2.508(2) Å. Each 2,3′-tmbpt links three Cu(II) ions to generate a tube-like chain with diameter of ca. 11 Å. The $[SiW_{12}O_{40}]^{4-}$-1 are located in the large cavity through

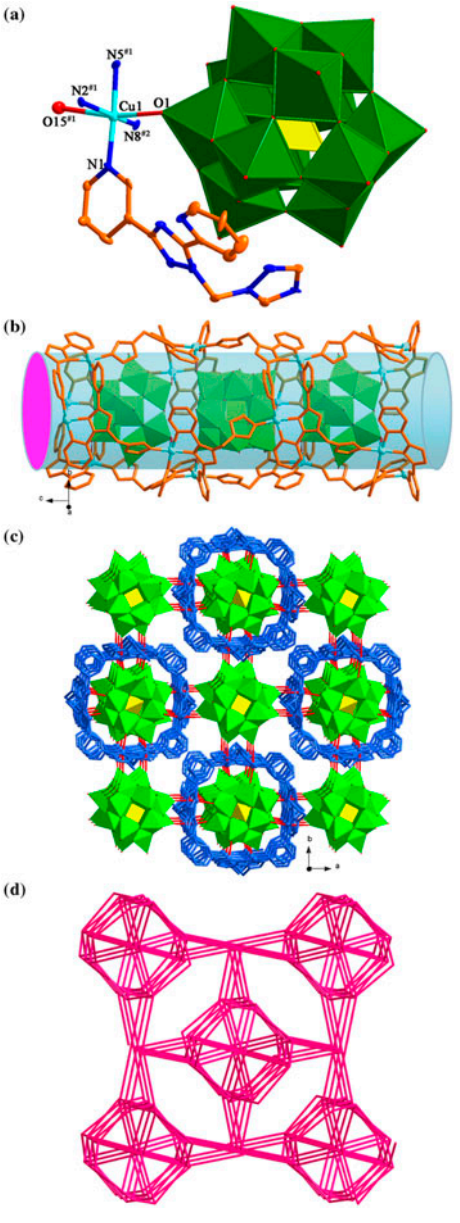

Figure 2. (a) Coordination environment of Cu(II) in **2** with hydrogens and lattice waters omitted for clarity. Symmetry codes: $^{\#1}y-1/2, x+1/2, -z+3/2$; $^{\#2}y-1/2, -x, -z+1$. (b) View of the chain formed by the Cu(II) ions, 2,3′-tmbpt ligands and $[SiW_{12}O_{40}]^{4-}$-1. (c) View of the 3-D framework of **2**. (d) Schematic view of the 3-D (3,4,5)-connected framework of **2** with $(4\cdot8^2)(4^4\cdot6^2)(8^4\cdot16^2)(4^3\cdot6^2\cdot8^3\cdot10^2)$ topology.

Cu–O bonds [figure 2(b)]. The $[SiW_{12}O_{40}]^{4-}$-2 are tetradentate linkages linking the chains to form a complicated 3-D framework [figure 2(c)].

Topologically, if 2,3′-tmbpt can be viewed as three-connected nodes, the $[SiW_{12}O_{40}]^{4-}$ can be regarded as two types of four-connected nodes, and the Cu(II)

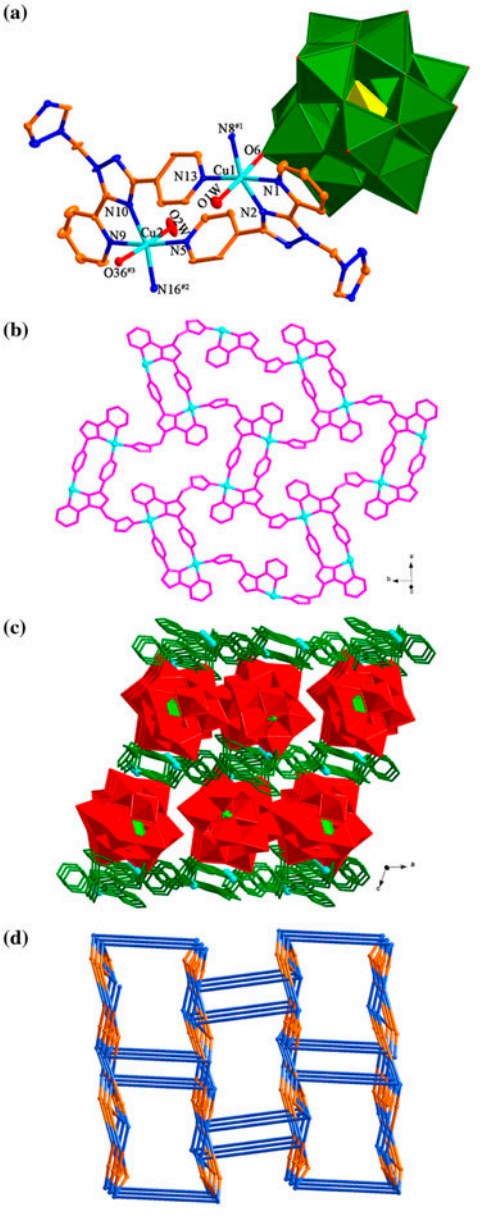

Figure 3. (a) Coordination environments of Cu(II) in **3** with hydrogens and lattice waters omitted for clarity. Symmetry codes: $^{\#1}-x+1/2,\ y+1/2,\ -z+1/2$; $^{\#2}-x+3/2,\ y-1/2,\ -z+1/2$; $^{\#3}x+1/2,\ -y+1/2,\ z-1/2$. (b) View of the layer formed by Cu(II) and 2,4′-tmbpt. (c) View of the 3-D framework of **3**. (d) Schematic view of the 3-D (3,4)-connected framework of **3** with $(4\cdot6\cdot8)(4\cdot6^2\cdot8^3)$ topology.

ions can be considered as five-connected nodes, the whole 3-D framework can be simplified as a (3,4,5)-connected net with $(4\cdot8^2)(4^4\cdot6^2)(8^4\cdot16^2)(4^3\cdot6^2\cdot8^3\cdot10^2)$ topology [figure 2(d)].

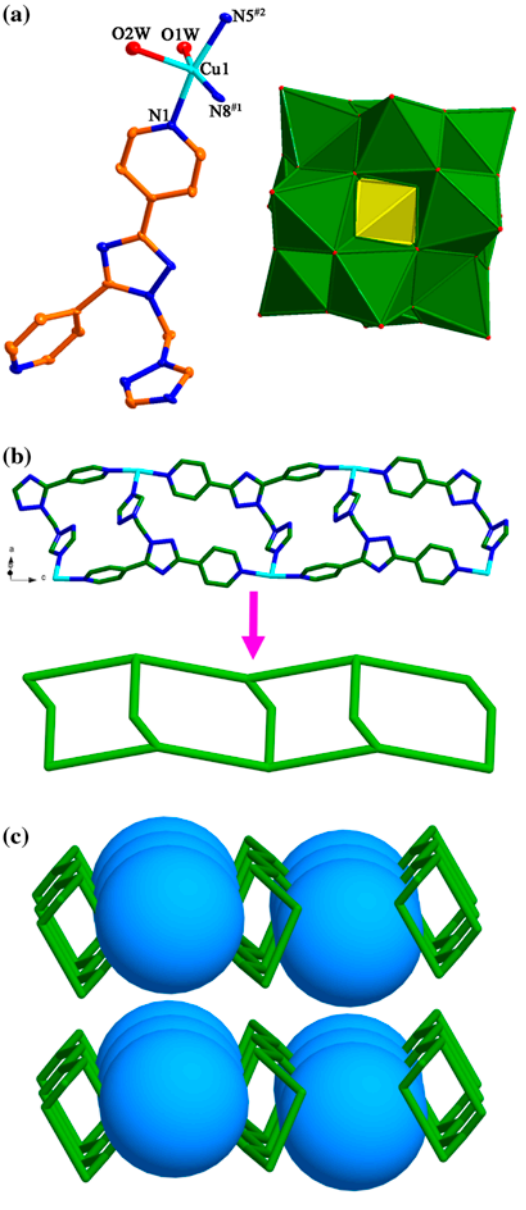

Figure 4. (a) Coordination environment of Cu(II) in **4** with hydrogens and lattice waters omitted for clarity. Symmetry codes: $^{\#1}-x, -y+1, -z$; $^{\#2}x, y, z+1$. (b) View of the chain formed by Cu(II) and 4,4′-tmbpt. (c) Schematic view of the 3-D supramolecular architecture of **4** (hydrogen bonds are omitted for clarity).

3.1.3. Crystal structure of $[Cu_2(2,4'\text{-tmbpt})_2(SiW_{12}O_{40})(H_2O)_2]\cdot 6.5H_2O$ (3). Compound **3** displays a 3-D (3,4)-connected framework with $(4\cdot6\cdot8)(4\cdot6^2\cdot8^3)$ topology. The asymmetric unit of **3** contains two Cu(II) ions, two 2,4′-tmbpt, one $[SiW_{12}O_{40}]^{4-}$, and eight and a half waters. As shown in figure 3(a), the Cu(II) ions have octahedral coordination geometries, defined by four nitrogens from three different 2,4′-tmbpt and two oxygens from one

$[SiW_{12}O_{40}]^{4-}$ and one water. The Cu–N bond lengths are 1.993(9)–2.059(7) Å and the Cu–O bond distances are 2.260(9)–2.609(9) Å. Each 2,4′-tmbpt links three Cu(II) ions to form 2-D layers [figure 3(b)], which are further linked by $[SiW_{12}O_{40}]^{4-}$ to generate an interesting 3-D framework [figure 3(c)].

Topologically, if the 2,4′-tmbpt ligands are three-connected nodes, the Cu(II) ions are four-connected nodes, and $[SiW_{12}O_{40}]^{4-}$ anions are viewed as linkers, the whole 3-D framework of **3** can be simplified as a (3,4)-connected net with $(4\cdot6\cdot8)(4\cdot6^2\cdot8^3)$ topology [figure 3(d)].

3.1.4. Crystal structure of $[Cu_2(4,4'\text{-tmbpt})_2(SiW_{12}O_{40})_0(H_2O)_4]\cdot13.5H_2O$ (4). Compound **4** shows a 3-D supramolecular architecture formed by hydrogen-bonding interactions among Cu(II) chains, $[SiW_{12}O_{40}]^{4-}$, and waters. The asymmetric unit of **4** consists of one Cu(II), one 4,4′-tmbpt, half a $[SiW_{12}O_{40}]^{4-}$, and eight and three quarters waters. As shown in figure 4(a), Cu1 is five-coordinate by three nitrogens from three different 4,4′-tmbpt ligands and two oxygens from two waters. Cu–N bond distances are 2.005(7)–2.020(6) Å and Cu–O bond distances are 1.981(6) and 2.173(7) Å. Each 4,4′-tmbpt bridges three Cu(II) ions to generate a ladder-like chain [figure 4(b)]. The chains and the $[SiW_{12}O_{40}]^{4-}$ anions are linked by O–H···O hydrogen-bonding interactions to form a 3-D supramolecular architecture [figure S1, figure 4(c) and table S4(b)].

3.1.5. Crystal structure of $[Cu(4,4'\text{-Htmbpt})(4,4'\text{-tmbpt})(PW_{12}O_{40})(H_2O)_2]\cdot7H_2O$ (5). Compound **5** shows an unusual 1-D→3-D interdigitated architecture. The asymmetric unit of **5** consists of two kinds of Cu(II) ions, one 4,4′-tmbpt, one protonated 4,4′-Htmbpt, one $[PW_{12}O_{40}]^{3-}$, and nine waters. As shown in figure 5(a), Cu1 and Cu2 are six-coordinate in octahedral coordination geometries, Cu1 by two nitrogens from two 4,4′-Htmbpt ligands and four oxygens from two $[PW_{12}O_{40}]^{3-}$ anions with two waters. Cu2 is coordinated by two nitrogens from two 4,4′-tmbpt ligands and four oxygens from two $[PW_{12}O_{40}]^{3-}$ anions, also with two waters. Cu–N bond lengths are 1.975(2)–2.047(2) Å and Cu–O bond lengths 1.991(2)–2.376(2) Å. Each $[PW_{12}O_{40}]^{3-}$ anion bridges two Cu(II) ions to yield 1-D chains, which are decorated by 4,4′-tmbpt and 4,4′-Htmbpt [figure 5(b)]. The uncoordinated pyridyl groups serve as dangling arms and thread into adjacent chains, resulting in an unusual 1-D→3-D interdigitated architecture [figure 5(c)]. Most reported interdigitated examples are related to highly undulating layers containing small and cramped windows involving protruding side arms [13]. However, the 3-D interdigitated architecture of **5** assembled from a 1-D chain is rarely observed in entangled systems [14].

Moreover, there are intermolecular N–H···N and O–H···O hydrogen-bonding interactions, which further consolidate the whole 3-D interdigitated architecture [figure S2 and table S5(b)].

Although **4** and **5** were constructed by the same 4,4′-tmbpt ligand and Cu(II), their structures are entirely different. The different coordination modes of the polyoxoanions lead to the structure difference of **4** and **5**. In **4**, $[SiW_{12}O_{40}]^{4-}$ is free, whereas the $[PW_{12}O_{40}]^{3-}$ in **5** serves as a bidentate ligand.

3.2. *Effects of the N-donor ligands on the structures of the compounds*

From the structural descriptions above, the N-donor ligands play important roles in the formation of resultant structures. Four N-donor ligands, such as 2,2′-tmbpt, 2,3′-tmbpt,

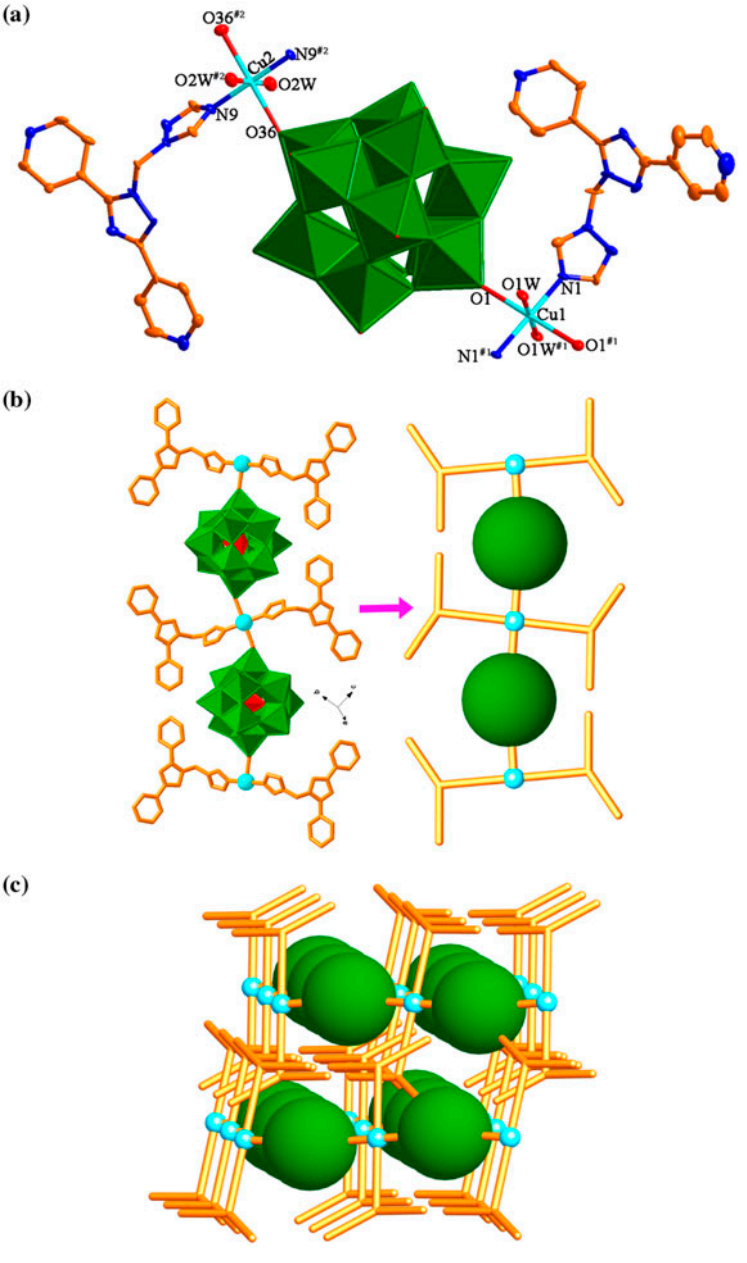

Figure 5. (a) Coordination environments of Cu(II) in **5** with hydrogens and lattice waters omitted for clarity. Symmetry codes: $^{\#1}-x+1, -y+1, -z+2$; $^{\#2}-x+2, -y, -z+1$. (b) View of the chain of **5**. (c) Schematic view of the 1-D→3-D interdigitated framework of **5**.

2,4′-tmbpt, and 4,4′-tmbpt, were used to investigate the effects of positions of the pyridyl-N on the structures. Compounds $[Cu_2(2,2'\text{-tmbpt})_2(SiW_{12}O_{40})]\cdot 9H_2O$ (**1**), $[Cu_2(2,3'\text{-tmbpt})_2(SiW_{12}O_{40})]\cdot 6H_2O$ (**2**), and $[Cu_2(2,4'\text{-tmbpt})_2(SiW_{12}O_{40})(H_2O)_2]\cdot 6.5H_2O$ (**3**) show

the effects of positions of the pyridyl-N atoms on the complex structures. In **1**–**3**, the pyridyl-N of tmbpt ligands are 2,2′-, 2,3′-, and 2,4′-positions, respectively. The three tmbpt ligands contain the same 2-position pyridyl-N, which can chelate one Cu(II) with the adjacent 4-position N atom of the central triazolyl ring (scheme 2). However, the remaining pyridyl-N on the 2′-(2,2′-tmbpt), 3′-(2,3′-tmbpt), and 4′-positions (2,4′-tmbpt) can freely rotate along the axes through the centers of the central triazolyl and pyridyl rings (scheme 2). Although the 4′-position pyridyl-N of 2,4′-tmbpt can freely rotate along the axis, it can only coordinate with metal ion on the axis. For the remaining 2′-position pyridyl-N of 2,2′-tmbpt, it is difficult to coordinate with metal ion because of steric hindrance. Compared with the 2′- and 4′-position pyridyl-N, the 3′-position pyridyl-N of 2,3′-tmbpt is flexible when coordinated with metal (scheme 2). The different positions of the pyridyl-N resulted in different Cu-tmbpt structures of **1**–**3**. In **1**, each 2,2′-tmbpt coordinates with two metal ions to form a highly undulated chain,

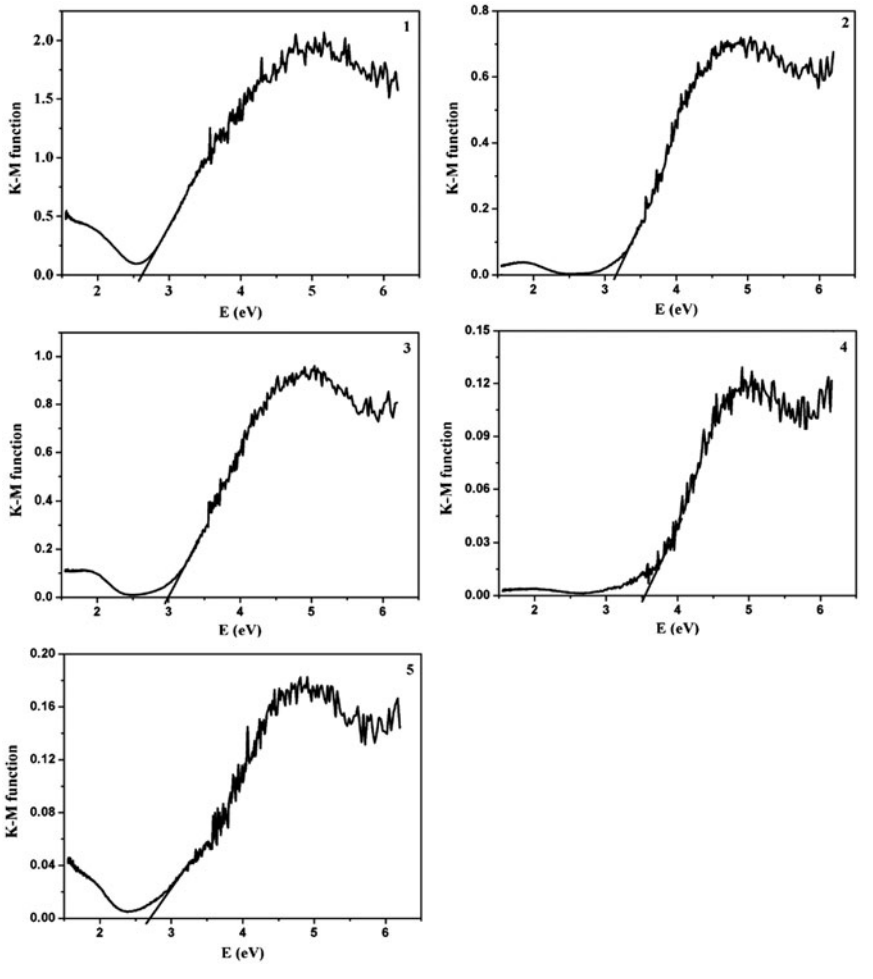

Figure 6. Kubelka-Munk-transformed diffuse reflectance spectra of **1**–**5**.

where the 2′-position pyridyl-N is free. In **2**, the flexible 2,3′-tmbpt ligands bridge the Cu(II) to form a tube-like chain structure. However, in **3**, the 2,4′-tmbpt ligands link Cu (II) ions to yield a 2-D layer structure.

The effects of the pyridyl-N on the complex structures are also supported by the structure difference between **3** and **4**. In **3**, the pyridyl groups in the 2,4′-tmbpt ligand are on the 2,4′-positions, while in **4**, the pyridyl groups in the 4,4′-tmbpt ligand are at the 4, 4′-positions. The 2-position pyridyl of the 2,4′-tmbpt can easily chelate one Cu(II) with the adjacent 4-position N of the central triazolyl ring. Thus, the 2,4′-tmbpt can be both chelating and bridging. However, 4,4′-tmbpt only is a bridging ligand. In **3**, 2,4′-tmbpt as both chelating and bridging links the Cu(II) ions to yield a 2-D layer structure. However, in **4**, the 4,4′-tmbpt as bridging connects Cu(II) ions to form a double chain. Clearly, position differences of the pyridyl-N in tmbpt ligands significantly influence the structures of the compounds.

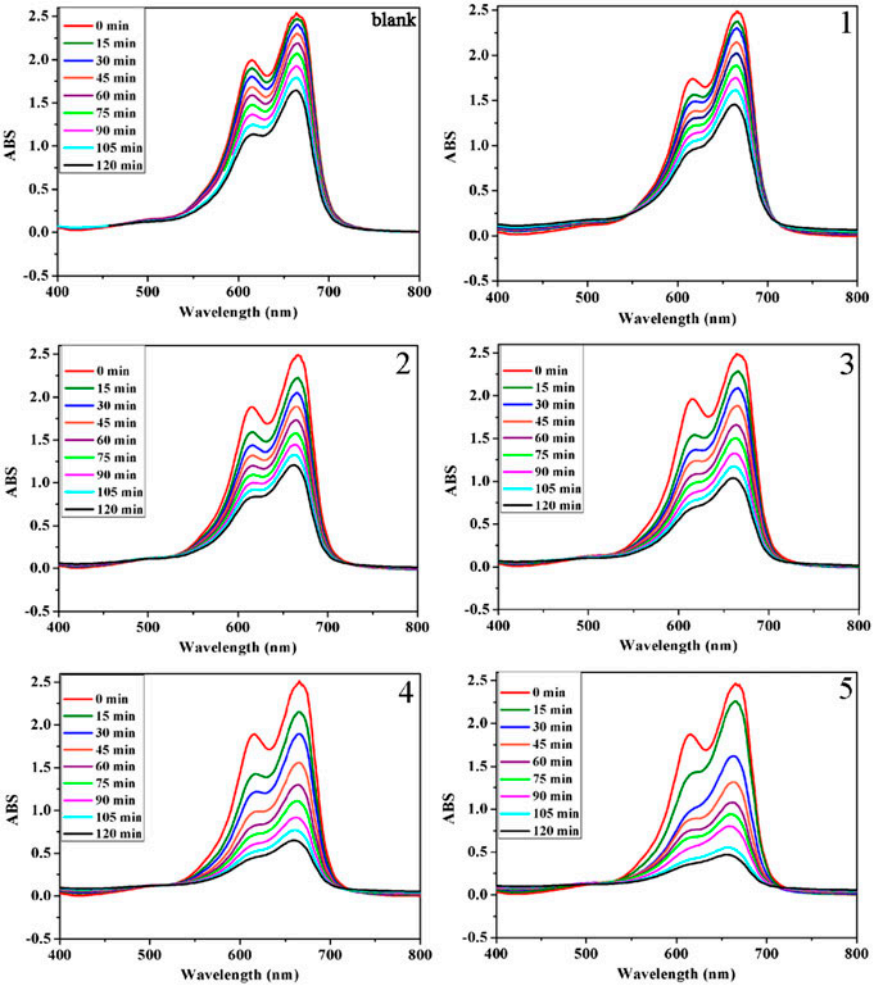

Figure 7. Absorption spectra of the MB solution during decomposition under UV light irradiation without catalysts (blank) and with **1**–**5**.

3.3. *IR spectra*

The O–H stretching vibrations of water in **1**–**5** are observed at 3446, 3547, 3414, 3566, and 3588 cm^{-1}, respectively [8h, 9c, 15]. In spectra of **1**–**5**, bands at 1063, 969, 881, and 790 cm^{-1} for **1**, 1065, 967, 880, and 760 cm^{-1} for **2**, 1067, 971, 876, and 777 cm^{-1} for **3**, 1066, 975, 850, and 759 cm^{-1} for **4**, and 1061, 957, 881, and 809 cm^{-1} for **5** are assigned to $\nu(X–O_a)$, $\nu(W=O_d)$, $\nu(W–O_b–W)$, and $\nu(W–O_c–W)$, respectively (X=Si for **1**–**4** and P for **5**) [16]. Bands at 1123–1612 cm^{-1} for **1**, 1130–1612 cm^{-1} for **2**, 1124–1618 cm^{-1} for **3**, 1122–1620 cm^{-1} for **4,** and 1102–1636 cm^{-1} for **5** are attributed to tmbpt ligands [16].

3.4. *PXRD results*

To confirm whether the crystal structures are truly representative of the bulk materials, PXRD experiments were performed for **1**–**5**. The PXRD patterns for the as-synthesized bulk materials are in agreement with the simulated ones from the single-crystal structure analyses, indicating pure solid-state phases (figures S3–S7 in Supplementary material see online supplemental material at http://dx.doi.org/10.1080/0000958972.2014.882503).

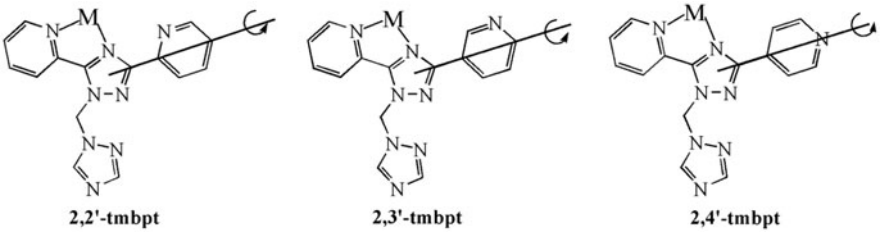

Scheme 2. View of the rotation axes of 2,2′-tmbpt, 2,3′-tmbpt, and 2,4′-tmbpt.

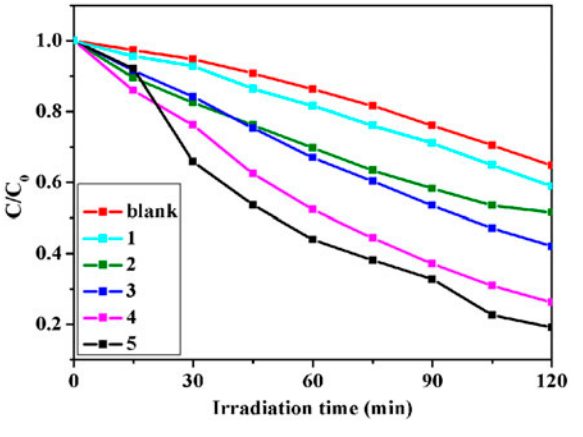

Figure 8. Changes in C/C_0 plots of MB solutions (5×10^{-5} ML^{-1}) *vs.* reaction time without catalysts (blank) and in the presence of **1**–**5**.

3.5. *Optical band gaps*

UV–Vis absorption spectra of **1**–**5** were measured in the crystalline state at room temperature (figure S8). Bands from 230 to 270 nm for **1**–**4** and 235–280 nm for **5** may be attributed to the O→W charge transfers [17].

A large number of POM-based inorganic–organic hybrid compounds have been reported to be potential semiconductor materials [18]. In this work, the diffuse reflectance spectra for **1**–**5** were performed to obtain their band gaps (E_g). The band gap was determined as the intersection point between the energy axis and the line extrapolated from the linear portion of the adsorption edge in a plot of Kubelka-Munk function F against E [19]. Kubelka-Munk function, $F=(1–R)^2/2R$, was transformed from the diffuse reflectance data, where R is the reflectance of an infinitely thick layer at a given wavelength. The F against E plots is shown in figure 6, and the E_g values of **1**–**5** are 2.62, 3.17, 3.00, 3.54, and 2.71 eV, respectively. The results reveal that **1**–**5** are potential semiconductor materials.

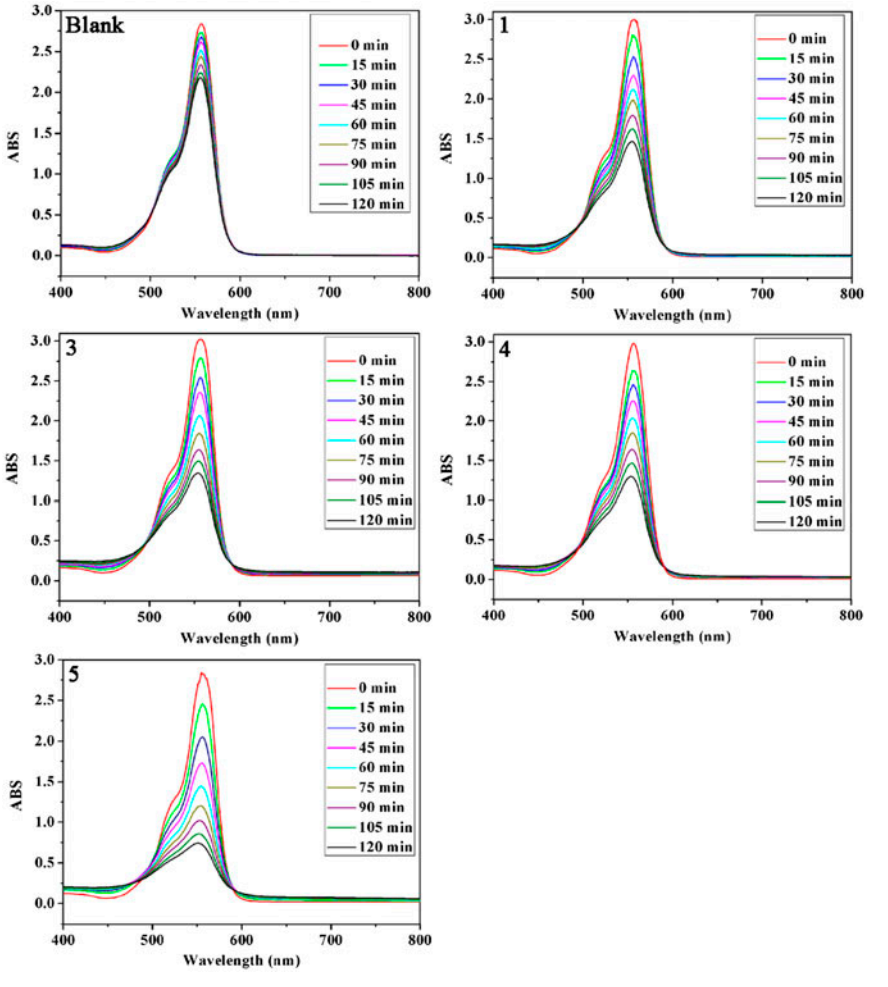

Figure 9. Absorption spectra of the RhB solution during decomposition under UV light irradiation without catalysts (blank) and with the use of the compounds.

3.6. *Photocatalytic properties*

Photocatalysis is an attractive property for POMs because of potential applications in decomposition of air and water contaminants [3f, 18]. MB and RhB, which are typically difficult to decompose in waste water [19], were employed to study the photocatalytic activities of **1**–**5**. Absorption spectra of the MB and RhB solution during the decomposition reaction under UV light irradiation without catalysts (blank) and with the use of **1**–**5** are shown in figure 7.

The absorption peaks of MB solution decreased for **1**–**5** after 120 min of irradiation. Changes in C/C_0 of MB solutions *versus* reaction time are plotted in figure 8. Photocatalytic activities increased from 35 (blank) to 41% for **1**, 51% for **2**, 58% for **3**, 74% for **4,** and 81% for **5**. After the photocatalytic processes, the colors of the MB solution became faint, indicating degradation of MB (figure S10 in Supplementary material). The results reveal that **1**–**5** have photocatalytic activities for degradation of MB. Photostabilities of **1**–**5** during the photocatalytic processes were monitored by PXRD patterns. The PXRD patterns are almost identical to those of the original compounds (figures S3–S7), indicating that **1**–**5** are stable during the photocatalytic processes. The results also imply that **1**–**5** can be used as stable photocatalysts for photodegradation of MB.

Photodegradation reactions of RhB upon 125 W Hg lamp irradiation employing **1** and **3**–**5** as the photocatalysts have been examined by UV–Vis spectroscopy. As shown in figure 9, after 120 min of irradiation, the absorption peaks of RhB solution decreased. The C/C_0 plots of RhB solution (4×10^{-5} mL^{-1}) *versus* reaction time are shown in figure 10, from which it can be found that the photocatalytic activities increased from 23 (blank) to 51% for **1**, 55% for **3**, 56% for **4,** and 74% for **5**. As for MB solution, changes in color of the RhB solution after the photocatalytic processes further implied the degradation of RhB (figure S11 in Supplementary material). The results reveal that **1** and **3**–**5** have photocatalytic activities for degradation of RhB. PXRD patterns of the compounds after the photocatalytic processes were nearly identical to those of the original compounds (figures S3–S7). Thus, **1** and **3**–**5** maintain their structural integrities

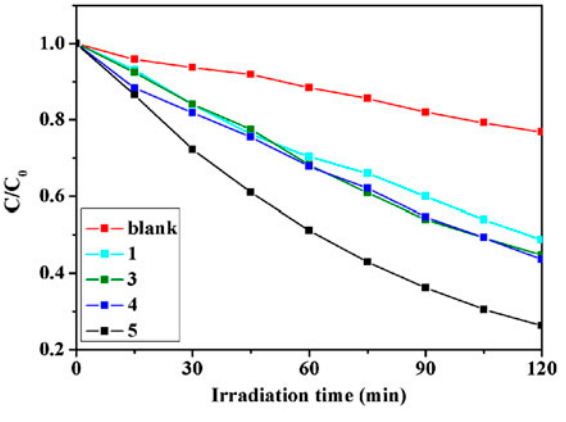

Figure 10. Changes in C/C_0 plots of RhB solutions (4×10^{-5} ML^{-1}) *vs.* reaction time without catalysts (blank) and in the presence of the compounds.

after photocatalysis, confirming that their stabilities toward photocatalysis are good. As heterogeneous photocatalysts, the POM-based compounds possess the features of simultaneous adsorption of both reactants (dioxygen and organic substrates dissolved in the reaction mixture) on the surface of catalysts and absorption of suitable light energy. The photocatalytic process happened on the surface of the catalysts (in the adsorbed phase), and the model of activation of the catalyst is photonic activation by exciting the POM with light energy higher than the band gap of POM, which results in an intramolecular O(2p)→W(5d) charge transfer and the formation of the excited state species (POM) [20]. For both MB and RhB, the photocatalysts did not show high photocatalytic activities. This may arise from weak π–π interactions between phenyl rings of MB and RhB and nitrogen heterocyclic rings of the photocatalysts, enhancing the chemical stabilities of MB and RhB in the solutions and slowing the photodegradation processes [21].

4. Conclusion

Five inorganic–organic hybrid compounds based on Keggin polyanions, Cu(II), and multidentate N-donors have been prepared under hydrothermal conditions. These compounds show 2-D and 3-D structures and interesting 1-D→3-D interdigitated architecture. The diverse structures of the compounds indicate that the N-donors play an important role in the formation of POM-based compounds. The tmbpt ligands are good candidates for the construction of POM-supported compounds with diverse structures. The optical band gaps of the compounds reveal that these compounds are potential semiconductor materials. The degradation rate curves of RhB for the four compounds are nearly linear, and the degradation rates are higher than 14% per hour, which are higher than a recently reported $[SiW_{12}O_{40}]^{4-}$-based compound $[Cu^{I}Bbi]_4SiW_{12}O_{40}\cdot H_2O$ [Bbi = 1,1-(1,4-butanediyl)-bis(imidazole)] [2h]. The photocatalytic behaviors of the compounds indicate that they may be stable photocatalysts for the photodegradation of MB and RhB.

Supplementary material

X-ray crystallographic files (CIF), PXRD patterns, selected bond lengths and angles, UV–Vis spectra, some related figures and TGA of the compounds. Crystallographic data for the structures reported in this article have been deposited with the Cambridge Crystallographic Data Center, CCDC Nos. 891260-891263 and 901610. Supplementary data associated with this article can be found in the online version.

Acknowledgements

We gratefully acknowledge the financial support from the National Natural Science Foundation of China (21202058), the Natural Science Foundation of Jiangsu Province (BK2011408), the Opening Project of Key Laboratory for Chemistry of Low-Dimensional Materials of Jiangsu Province (JSKC12109), and the Cultivation Fund of the Key Scientific Innovation Project of Huaiyin Normal University (11HSGJBZ11).

Funding

This research was supported by the National Science Foundation of China [grant number 41272240]; China Geological Survey project [grant number 1212011221093]; [grant number 12120113036700].

References

[1] (a) S.T. Zheng, J. Zhang, X.X. Li, W.H. Fang, G.Y. Yang. *J. Am. Chem. Soc.*, **132**, 15102 (2010); (b) S. Uchida, R. Eguchi, N. Mizuno. *Angew. Chem. Int. Ed.*, **49**, 9930 (2010); (c) X.K. Fang, P. Kögerler, L. Isaacs, S. Uchida, N. Mizuno. *J. Am. Chem. Soc.*, **131**, 432 (2009); (d) A. Dolbecq, E. Dumas, C.R. Mayer, P. Mialane. *Chem. Rev.*, **110**, 6009 (2010); (e) D.L. Long, R. Tsunashima, L. Cronin. *Angew. Chem. Int. Ed.*, **49**, 1736 (2010); (f) U. Kortz, A. Müller, J.V. Slageren, J. Schnacke, N.S. Dalalf, M. Dressel. *Coord. Chem. Rev.*, **253**, 2315 (2009); (g) R. Yang, S.X. Liu, Q. Tang, S.J. Li, D.D. Liang. *J. Coord. Chem.*, **65**, 891 (2012); (h) J.Q. Sha, L.J. Sun, E.L. Zheng, H.B. Qiu, M.Y. Liu, H. Zhao, H. Yuan. *J. Coord. Chem.*, **66**, 602 (2013).

[2] (a) S.T. Zheng, J. Zhang, G.Y. Yang. *Angew. Chem. Int. Ed.*, **47**, 3909 (2008); (b) A. Yokoyama, T. Kojima, K. Ohkubo, S. Fukuzumi. *Chem. Commun.*, **39**, 3997 (2007); (c) C. Streb, C. Ritchie, D.L. Long, P. Kögerler, L. Cronin. *Angew. Chem. Int. Ed.*, **46**, 7579 (2007); (d) V. Shivaiah, M. Nagaraju, S.K. Das. *Inorg. Chem.*, **42**, 6604 (2003); (e) L. Yang, L.L. Hou, P.T. Ma, J.Y. Niu. *J. Coord. Chem.*, **66**, 1330 (2013); (f) A.X. Tian, X.L. Lin, Y.J. Liu, G.Y. Liu, J. Ying, X.L. Wang, H.Y. Lin. *J. Coord. Chem.*, **65**, 2147 (2012); (g) X.Y. Liu, H.L. Nie, L. Wang, R.D. Huang. *J. Coord. Chem.*, **66**, 444 (2013); (h) X. Gan, X.X. Hu, Z.F. Shi, Y.Z. Yin. *J. Coord. Chem.*, **66**, 2930 (2013).

[3] (a) J.Q. Sha, J. Peng, H.S. Liu, J. Chen, B.X. Dong, A.X. Tian, Z.M. Su. *Eur. J. Inorg. Chem.*, **46**, 1268 (2007); (b) Q.G. Zhai, X.Y. Wu, S.M. Chen, Z.G. Zhao, C.Z. Lu. *Inorg. Chem.*, **46**, 5046 (2007); (c) R.G. Cao, S.X. Liu, L.H. Xie, Y.B. Pan, J.F. Cao, Y.H. Ren, L. Xu. *Inorg. Chem.*, **46**, 3541 (2007); (d) R.P. Bontchev, E.L. Venturini, M. Nyman. *Inorg. Chem.*, **46**, 4483 (2007); (e) A.X. Tian, J. Ying, J. Peng, J.Q. Sha, Z.G. Han, J.F. Ma, Z.M. Su, N.H. Hu, H.Q. Jia. *Inorg. Chem.*, **47**, 3274 (2008); (f) H.S. Lin, P.A. Maggard. *Inorg. Chem.*, **47**, 8044 (2008); (g) H.X. Yang, S.Y. Gao, J. Lu, B. Xu, J.X. Lin, R. Cao. *Inorg. Chem.*, **49**, 736 (2010).

[4] (a) R.M. Yu, X.F. Kuang, X.Y. Wu, C.Z. Lu, J.P. Donahue. *Coord. Chem. Rev.*, **253**, 2872 (2009); (b) D. Hagrman, C. Zubieta, D.J. Rose, J. Zubieta, R.C. Haushalter. *Angew. Chem. Int. Ed.*, **38**, 3165 (1999); (c) S.T. Zheng, G.Y. Yang. *Dalton Trans.*, 700 (2010); (d) C.Y. Duan, M.L. Wei, D. Guo, C. He, Q.J. Meng. *J. Am. Chem. Soc.*, **132**, 3321 (2010); (e) C.Y. Sun, S.X. Liu, D.D. Liang, K.Z. Shao, Y.H. Ren, Z.M. Su. *J. Am. Chem. Soc.*, **131**, 1883 (2009); (f) D.B. Dang, Y. Bai, C. He, J. Wang, C.Y. Duan, J.Y. Niu. *Inorg. Chem.*, **49**, 12802 (2010).

[5] (a) A.X. Tian, J. Ying, J. Peng, J.Q. Sha, Z.M. Su, H.J. Pang, P.P. Zhang, Y. Chen, M. Zhu, Y. Shen. *Cryst. Growth Des.*, **10**, 1104 (2010); (b) J. Wu, Y.L. Xu, K. Yu, Z.H. Su, B.B. Zhou. *J. Coord. Chem.*, **66**, 2821 (2013); (c) S.H. Yang, X.Q. Dong, Y.P. Zhang, H.M. Hu, G.L. Xue. *J. Coord. Chem.*, **66**, 1529 (2013).

[6] (a) A.Y. Robin, K.M. Fromm. *Coord. Chem. Rev.*, **250**, 2127 (2006); (b) A.J. Blake, N.R. Champness, P. Hubberstey, W.S. Li, M.A. Withersby, M. Schröder. *Coord. Chem. Rev.*, **183**, 117 (1999).

[7] (a) C. Ritchie, E. Burkholder, P. Kögerler, L. Cronin. *Dalton Trans.*, 1712 (2006); (b) L. Lisnard, A. Dolbecq, P. Mialane, J. Marrot, E. Codjovi, F. Sécheresse. *Dalton Trans.*, 3913 (2005); (c) J. Chen, S.F. Lu, R.M. Yu, Z.N. Chen, Z.X. Huang, C.Z. Lu. *Chem. Commun.*, **22**, 2640 (2002); (d) L.S. Felices, P. Vitoria, J.M. Gutiérrez-Zorrilla, L. Lezama, S. Reinoso. *Inorg. Chem.*, **45**, 7748 (2006).

[8] (a) S.L. Li, Y.Q. Lan, J.F. Ma, J. Yang, X.H. Wang, Z.M. Su. *Inorg. Chem.*, **46**, 8283 (2007); (b) Y.Q. Lan, S.L. Li, X.L. Wang, K.Z. Shao, Z.M. Su, E.B. Wang. *Inorg. Chem.*, **47**, 529 (2008); (c) X.L. Wang, C. Qin, E.B. Wang, Z.M. Su. *Chem. Commun.*, **41**, 4245 (2007); (d) Y.Q. Lan, S.L. Li, X.L. Wang, K.Z. Shao, D.Y. Du, H.Y. Zang, Z.M. Su. *Inorg. Chem.*, **47**, 8179 (2008); (e) A.X. Tian, J. Ying, J. Peng, J.Q. Sha, H.J. Pang, P.P. Zhang, Y. Chen, M. Zhu, Z.M. Su. *Cryst. Growth Des.*, **8**, 3717 (2008); (f) C. Qin, X.L. Wang, L. Yuan, E.B. Wang. *Cryst. Growth Des.*, **8**, 2093 (2008); (g) S.L. Li, Y.Q. Lan, J.F. Ma, J. Yang, J. Liu, Y.M. Fu, Z.M. Su. *Dalton Trans.*, 2015 (2008); (h) J.X. Meng, Y. Lu, Y.G. Li, H. Fu, E.B. Wang. *Cryst. Growth Des.*, **9**, 4116 (2009); (i) B.X. Dong, Q. Xu. *Inorg. Chem.*, **48**, 5861 (2009).

[9] (a) R.S.J. Rarig, J. Zubieta. *J. Chem. Soc., Dalton Trans.*, 3446 (2001); (b) H.Y. Liu, H. Wu, J.F. Ma, Y.Y. Liu, J. Yang, J.C. Ma. *Dalton Trans.*, 602 (2011); (c) H.Y. Liu, J. Yang, Y.Y. Liu, J.F. Ma. *Dalton Trans.*, 9922 (2012); (d) H.Y. Liu, B. Liu, J. Yang, Y.Y. Liu, J.F. Ma, H. Wu. *Dalton Trans.*, **40**, 9782 (2011).

[10] (a) W.Q. Kan, B. Liu, J. Yang, Y.Y. Liu, J.F. Ma. *Cryst. Growth Des.*, **12**, 2288 (2012); (b) W.R. Browne, C.M. O'Connor, H.P. Hughes, R. Hage, O. Walter, M. Doering, J.F. Gallagher, J.G. Vos. *J. Chem. Soc., Dalton Trans.*, 4048 (2002).

[11] (a) G.M. Sheldrick. *SHELXS-97, Programs for X-ray Crystal Structure Solution*, University of Göttingen, Göttingen, Germany (1997); (b) G.M. Sheldrick. *SHELXL-97, Programs for X-ray Crystal Structure Refinement*, University of Göttingen, Göttingen, Germany (1997).

[12] (a) M.G. Liu, P.P. Zhang, J. Peng, H.X. Meng, X. Wang, M. Zhu, D.D. Wang, C.L. Meng, K. Alimaje. *Cryst. Growth Des.*, **12**, 1273 (2012); (b) P.P. Zhang, J. Peng, J.Q. Sha, A.X. Tian, H.J. Pang, Y. Chen, M. Zhu. *CrystEngComm*, **11**, 902 (2009).
[13] (a) Y.N. Xia, S.G. Li, B. Wu, Y.Y. Liu, X.J. Yang. *CrystEngComm*, **13**, 5763 (2011); (b) L.F. Ma, L.Y. Wang, J.L. Hu, Y.Y. Wang, S.R. Batten, J.G. Wang. *CrystEngComm*, **11**, 777 (2009); (c) S.R. Batten, A.R. Harris, P. Jensen, K.S. Murray, A. Ziebell. *J. Chem. Soc., Dalton Trans.*, 3829 (2000); (d) H.D. Guo, X.M. Guo, S.R. Batten, J.F. Song, S.Y. Song, S. Dang, G.L. Zheng, J.K. Tang, H.J. Zhang. *Cryst. Growth Des.*, **9**, 1394 (2009); (e) E.Y. Choi, L.D. DeVries, R.W. Novotny, C. Hu, W. Choe. *Cryst. Growth Des.*, **10**, 171 (2010).
[14] (a) H. Chen, D. Xiao, L. Fan, J. He, S. Yan, G. Zhang, D. Sun, Z. Ye, R. Yuan, E. Wang. *CrystEngComm*, **13**, 7098 (2011); (b) W.Q. Kan, J.F. Ma, Y.Y. Liu, J. Yang. *CrystEngComm*, **14**, 2316 (2012).
[15] W.Q. Kan, J.F. Ma, Y.Y. Liu, H. Wu, J. Yang. *CrystEngComm*, **13**, 7037 (2011).
[16] (a) H.J. Pang, H.Y. Ma, J. Peng, C.J. Zhang, P.P. Zhang. *CrystEngComm*, **13**, 7079 (2011); (b) A.X. Tian, J. Ying, J. Peng, J.Q. Sha, H.J. Pang, P.P. Zhang, Y. Chen, M. Zhu, Z.M. Su. *Inorg. Chem.*, **48**, 100 (2009); (c) D.Y. Du, J.S. Qin, G. Yuan, Y.Q. Lan, X.L. Wang, K.Z. Shao, Z.M. Su. *Solid State Sci.*, **13**, 1115 (2011).
[17] (a) D. Rusu, C. Rosu, C. Crăciun, L. David, M. Rusu, Gh. Marcu. *J. Mol. Struct.*, **563–564**, 427 (2001); (b) T. Yamase. *Chem. Rev.*, **98**, 307 (1998).
[18] (a) Y. Guo, Y. Wang, C. Hu, Y. Wang, E. Wang, Y. Zhou, S. Feng. *Chem. Mater.*, **12**, 3501 (2000); (b) A. Mylonas, A. Hiskia, E. Papaconstanitinou. *J. Mol. Catal. A: Chem.*, **114**, 191 (1996); (c) Y. Hu, F. Luo, F. Dong. *Chem. Commun.*, **47**, 761 (2011); (d) Q. Wu, W.L. Chen, D. Liu, C. Liang, Y.G. Li, S.W. Lin, E. Wang. *Dalton Trans.*, 56 (2011).
[19] (a) B. Liu, Z.T. Yu, J. Yang, H. Wu, Y.Y. Liu, J.F. Ma. *Inorg. Chem.*, **50**, 8967 (2011); (b) P.P. Zhang, J. Peng, H.J. Pang, J.Q. Sha, M. Zhu, D.D. Wang, M.G. Liu, Z.M. Su. *Cryst. Growth Des.*, **11**, 2736 (2011).
[20] (a) H. Fu, Y. Li, Y. Lu, W. Chen, Q. Wu, J. Meng, X. Wang, Z. Zhang, E. Wang. *Cryst. Growth Des.*, **11**, 458 (2011); (b) Y.H. Guo, Y.H. Wang, C.W. Hu, Y.H. Wang, E.B. Wang. *Chem. Mater.*, **12**, 3501 (2000); (c) C.C. Chen, W. Zhao, P.X. Lei, J.C. Zhao, N. Serpone. *Chem. Eur. J.*, **10**, 1956 (2004).
[21] J.Y. Niu, S.W. Zhang, H.N. Chen, J.W. Zhao, P.T. Ma, J.P. Wang. *Cryst. Growth Des.*, **11**, 3769 (2011).